ResearchGate

See discussions, stats, and author profiles for this publication at: https://www.researchgate.net/publication/237764578

# Semiclassical Calculations on the Energy Dependence of the Steric Effect for the Reactions Ca ( 1 D ) + CH 3 X ( jkm = 111) → CaX + CH 3 with X = F, Cl, Br

**ARTICLE** *in* THE JOURNAL OF PHYSICAL CHEMISTRY · OCTOBER 1996

Impact Factor: 2.78 · DOI: 10.1021/jp961584n

CITATIONS
10

READS
5

**3 AUTHORS**, INCLUDING:

Anthony J. H. M. Meijer
The University of Sheffield
**97** PUBLICATIONS **1,518** CITATIONS
SEE PROFILE

Ad van der Avoird
Radboud University Nijmegen
**288** PUBLICATIONS **7,262** CITATIONS
SEE PROFILE

Available from: Anthony J. H. M. Meijer
Retrieved on: 04 February 2016

# Semiclassical Calculations on the Energy Dependence of the Steric Effect for the Reactions Ca ($^1D$) + $CH_3X$ ($jkm = 111$) → CaX + $CH_3$ with X = F, Cl, Br

**Anthony J. H. M. Meijer,* Gerrit C. Groenenboom, and Ad van der Avoird**

*Institute of Theoretical Chemistry, NSR Center, University of Nijmegen, Toernooiveld, 6525 ED Nijmegen, The Netherlands*

*Received: May 30, 1996; In Final Form: July 30, 1996*[⊗]

In this article we investigate the energy dependence of the steric effect for the title reactions with X = F, Cl, and Br and CaX in the excited states $A^2\Pi$, $B^2\Sigma^+$, and $A'^2\Delta$. We use a semiclassical method (Meijer, A. J. H. M.; Groenenboom, G. C.; van der Avoird, A. *J. Chem. Phys.* **1996**, *105*, 2247). The rotation of the $CH_3X$ molecule and the asymptotically degenerate electronic states of the interacting atom and molecule are treated quantum mechanically. To describe the reaction we use a model which correlates the projection of the electronic angular momentum on the intermolecular axis with the projection of the electronic orbital angular momentum on the diatomic axis (Menzinger, M. *Polon. Phys. Acta* **1988**, *A73*, 85). We conclude that with this model it becomes possible to reproduce and explain the observed *negative* steric effect for the Ca($^1D$) + $CH_3Cl$ ($jkm = 111$) → CaCl ($B^2\Sigma^+$) + $CH_3$. Furthermore, we conclude that the differences between the measured steric effects for the three reactions studied can be attributed to differences in the "cone of acceptance" for the three molecules studied. We find that the "cone of acceptance" increases when going from $CH_3F$ to $CH_3Cl$ or $CH_3Br$, as might be expected.

## 1. Introduction

There have been a number of studies into the role of reagent orientation in chemical reactions. One of the methods used to orient symmetric-top (like) molecules in such an experiment is the hexapole technique. In this method a hexapole field is used to select a certain rotational state, labeled by the symmetric top quantum numbers *j*, *k*, and *m*. A hexapole field combined with a homogeneous electric field allows control over the (average) spatial orientation (given by angle $\beta$) of the molecular symmetry axis with respect to the relative velocity of the colliding particles.[1−14] Other methods to control the orientation of molecules have been reported as well; see, e.g., refs 15−21.

In this article we focus on the experiments for Ca ($^1D$) + $CH_3X$ ($jkm = 111$) → CaX ($A^2\Pi$, $B^2\Sigma^+$, $A'^2\Delta$) + $CH_3$ with X equal to F, Cl, or Br by Janssen, Parker, and Stolte.[14,22] They measured the steric effect as a function of the relative translational energy for some of the exit channels for these reactions. The steric effect for the ($jkm = 111$) rotational state is defined as the difference between the reactive cross section for favorably oriented molecules (meaning that the X atom points toward the Ca atom) and the reactive cross section for unfavorably oriented molecules ($CH_3$ group first), normalized to the total reactive cross section for unoriented molecules. Only the CaF ($A^2\Pi$), the CaCl ($B^2\Sigma^+$), and the CaBr ($A^2\Pi$) exit channels were measured, because of experimental limitations.

Most theoretical studies on orientational effects in chemical reactions employ some version of the angle dependent line of centers (ADLC) model to describe the reaction probability. In the ADLC model the molecule is assumed to be surrounded by an energy barrier, visualized as an imaginary sphere. Atoms are only reactive if they have sufficient radial kinetic energy to surmount the barrier. One could take this barrier proportional to the cosine of the angle $\beta_R$ between the symmetry axis of the molecule and the intermolecular axis. From this model one predicts a decreasing steric effect for increasing translational energies, because at higher energies a wider range of angles $\beta_R$ is able to react. This behavior has been observed experimentally, e.g., for the Ba + $N_2O$ reaction.

For Ca + $CH_3F$ ($jkm = 111$) → CaF ($A^2\Pi$) + $CH_3$ Janssen *et al*. found an *increasing* steric effect with increasing energy. This result could not be explained using the ADLC model. It was tentatively explained in terms of reorientation of initially *unfavorably* oriented $CH_3F$ molecules towards the approaching Ca atom. Reorientation would scramble the initially prepared orientation and thereby lower the steric effect. At higher energies there would not be sufficient time for this reorientation to occur and the steric effect remains high. The reorientation was assumed to be caused by anisotropic terms in the long range interaction between a quadrupole moment on Ca and the permanent multipole moments on $CH_3X$. Although an isolated atom cannot have a permanent multipole moment, the electric field of the approaching molecule will split the fivefold degenerate $^1D$ state of Ca. This gives rise to five (asymptotically degenerate) substates, each of which has a quadrupole moment.

Another explanation for the observed steric effect was found in quasiclassical trajectory calculations on an isotropic model potential in paper 1.[23] As it turns out, atoms with large impact parameters will fly around the molecule and hit it at the back, thus counteracting the effect of the initially prepared orientation. We called this phenomenon "trapping". Trapping will decrease the steric effect. At higher energies these trajectories with large impact parameters will fly by the molecule and be nonreactive, thus increasing the steric effect.

In paper 2[24] we showed that quasiclassical trajectory calculations, using the long range potential defined above and the modified quasi classical trajectory (MQCT) approach from paper 1, confirm the importance of trapping. However, its effect is partly canceled by reorientation of initially *favorably* oriented molecules in such a way that they follow the approaching Ca atom, even if this atom is trapped and, without reorientation, would hit the molecule in the back. The cancellation of the effects of reorientation and trapping resulted in a steric effect that did not reproduce the experimental data.

[⊗] Abstract published in *Advance ACS Abstracts,* September 15, 1996.

S0022-3654(96)01584-5 CCC: $12.00 © 1996 American Chemical Society

Also a semiclassical (SC) method was developed to try to reproduce the experimentally observed steric effect (see paper 3[25]). In semiclassical methods some coordinates are treated classically using Hamilton's equations of motion. Other coordinates are treated quantum mechanically using the time-dependent Schrödinger equation. Hence, in our calculations a quantum mechanical wave function, describing the rotation of the molecule and the electronic degrees of freedom of the atom, and a classical particle, describing the relative motion of the colliding particles, are propagated simultaneously in time from 30 bohr to the harpooning radius at 6.0 bohr. Up to this point the scattering is assumed to be nonreactive but possibly inelastic. This SC method yielded better results than the MQCT approach in paper 2, but still did not yield agreement with experiment.

In the MQCT calculations and in the SC calculations it was assumed in first instance that the branching ratio for the different exit channels was energy independent (we called this the "uncorrelated model"). Later, in paper 3, we also introduced the "correlated model" (proposed by Menzinger in 1988[26,27]), which makes a different assumption. This model correlates the electronic angular momentum of the atom at the moment of reaction to the final electronic angular momentum of the product. Evidence for such a correlation has been found experimentally.[28−31] Using this model together with the SC method it became possible to reproduce the experimentally measured steric effect for the CaF ($A^2\Pi$) exit channel. Also predictions were made regarding the steric effect for the $B^2\Sigma^+$ and $A'^2\Delta$ exit channels.

In this article we want to examine the *negative* steric effect measured for Ca + $CH_3Cl$ ($jkm = 111$) → CaCl ($B^2\Sigma^+$) + $CH_3$. This negative steric effect cannot be explained using the standard ADLC model. Furthermore, we look at the Ca + $CH_3Br$ reaction, also measured by Janssen *et al.*[22] In section II we discuss the main physical ideas and models on which our calculations are based. In section III we give some computational details. In section IV we discuss the results for the Ca + $CH_3Cl$ and Ca + $CH_3Br$ reactions and compare them to the results of paper 3 on Ca + $CH_3F$ and to the experiment. We also give predictions for the exit channels that were not measured experimentally. Lastly, in section V we draw some conclusions regarding the differences between the three systems and regarding the accuracy of the methods used. Finally, we point out where we think that our calculations might be improved.

## II. Theory

For a detailed discussion of the theory used in this paper we refer to paper 3.[25] Here, we only give an outline and focus more on the underlying chemical and physical models and ideas.

In the experiments by Janssen *et al*. on the reactions between Ca and $CH_3X$,[22,14] Ca atoms in the $^1D$ state were used. This $^1D$ state is a metastable excited state of the Ca atom at 2.71 eV above the ground state. The lifetime of this state is approximately 1.7 ms [32] and it has a fivefold degeneracy. Its components with respect to the initial velocity vector (taken to be the *z*-axis of a space fixed (SF) frame) are labeled by the magnetic quantum number $\mu = -2, ..., 2$. However, the presence of an electric field from the molecule lifts this degeneracy and gives rise to 5 (adiabatic) substates, labeled by *N*. The electronic state of Ca is treated quantum mechanically in our calculations in order to include this "preparation" of the adiabatic states, as well as nonadiabatic energy transfer. We restrict the description of the electronic state of Ca to the five components of the $^1D$ state and of the $CH_3X$ molecule to its electronic ground state. We expand the interaction operator in a multipole series. Hence, we get an electrostatic long range potential in which the Ca atom is represented by the 5 × 5 quadrupole matrix of the $^1D$ state. The electronic state of the $CH_3X$ molecule enters the potential through the dipole moment $\langle Q_0^1 \rangle$, the quadrupole moment $\langle Q_0^2 \rangle$, and the octupole moment components $\langle Q_0^3 \rangle$ and $\langle Q_3^3 \rangle$. We wish to emphasize here that if we were to include also other interactions, such as induction or dispersion, we would have to include also other electronic states of Ca and $CH_3X$.

The $CH_3X$ molecules are treated in our calculations as rigid symmetric top molecules. Their rotational state is labeled by the symmetric top quantum numbers *j*, *k*, and *m*. The experiment prepares molecules in the $(j,k,m) = (1,1,1)$ state. We treat the rotation of the molecule during the collision quantum mechanically, because the quantum mechanical description of such a low *j*-state is totally different from the classical description. In the experiment the $CH_3X$ molecules are rotationally state selected by a hexapole field. Subsequently, they pass through two different homogeneous electric fields. The first field, the guiding field, orients the molecules in the laboratory frame and is used to ensure that the state selection is preserved between hexapole and reaction chamber. The second field, the harp field, is placed in the reaction chamber and orients the molecules with respect to the direction of the incoming atoms. In the experiment three different reaction geometries are used, in which the Ca atom always approaches from the $+z$-direction. In the first reaction geometry the C−X axis is preferentially oriented toward the approaching Ca atom. This will be called the favorable orientation. It corresponds to a calculation starting in a $(j, k, m) = (1,1,1)$ state. To obtain the second collision geometry, the direction of the homogeneous electric field is reversed. Hence, the C−X axis is preferentially oriented away from the approaching Ca atom. This will be called the unfavorable collision geometry. It corresponds to a calculation starting in a $(j, k, m) = (1, 1, -1)$ state. In the third collision geometry, the homogeneous electric field is switched off. The molecule will still be $(j, k)$ state selected, but its orientation with respect to the atom is now randomized. We perform additional calculations starting in a $(j, k, m) = (1, 1, 0)$ state and obtain the result for randomly oriented molecules as the average over the three calculations with $m = -1, 0, 1$.

The initial conditions for the calculations are labeled by $\kappa = (b, j_i, k_i, m_i, N_i)$, where *b* is the impact parameter for the collision, while $j_i$, $k_i$, and $m_i$ are the initial rotational states of the $CH_3X$ molecule. In our calculations $j_i$ and $k_i$ are always 1 and $m_i$ is 1, 0, or −1, as discussed above. Last, $N_i$ labels the initial (adiabatic) electronic state of the Ca atom. These states are defined to be the eigenvectors of the interaction matrix averaged over the initial orientational probability distribution of the $CH_3X$ molecule in the rotational state $(j_i, k_i, m_i)$. The states $N_i$ are constructed this way to ensure that the evolution of the electronic state of Ca is as adiabatic as possible, which makes the semiclassical method most reliable (see paper 3, section II.F). The states $N_i$ are *not* equal to the adiabatic states *N* of the Ca + $CH_3X$ systems, which would be a more obvious choice for the initial electronic states of the Ca atom. However, it is not possible to start in a pure adiabatic state *N* and at the same time in a pure rotational state $(j, k, m)$, because the adiabatic states are defined for a given orientation $(\alpha, \beta, \gamma)$ of the $CH_3X$ molecules, whereas in our calculations we deal with molecules that are initially in a pure quantum state $(j_i, k_i, m_i)$.

The relative motion of the colliding particles is described by classical mechanics in such a way that the total energy of the system is conserved during the collision.[25,33−39] However, microscopic reversibility is not obeyed; i.e., the probability of

an excitation from state $n$ to state $m$ is not equal to the probability of the reverse process. Methods have been published to circumvent this problem (see, e.g., refs 38 and 39). However, since the rotational energy is approximately 0.5% of the relative kinetic energy and since it never exceeds 4, reversibility will be small[39] and we have not implemented these methods.

During the collision we monitor three different phenomena: trapping, reorientation, and the evolution of the electronic state of Ca. Trapping is the phenomenon that an atom approaching the molecule with a large impact parameter can be "captured" by the potential. In that case, it will fly around the molecule and may collide with it at the "back". If this happens, the initially prepared orientation of the molecular symmetry axis with respect to the atom will be scrambled. The second effect is reorientation, which counteracts the effect of trapping. If it occurs, an initially favorably oriented C−X axis will rotate to follow the approaching atom until the two particles collide. The third phenomenon we investigate is the evolution of the electronic state of the Ca atom. In order to determine what model describes the electronic behavior best, we monitor the populations of the electronic states in three different representations. In the first representation we monitor the populations $Q_\mu^{(\kappa)}(t)$ of the diabatic $^1D$ substates, labeled by $\mu$, in the space fixed (SF) frame. In the second representation the $^1D$ substates, labeled by $\Lambda$, refer to the DF (dimer fixed) frame in which the intermolecular axis is the $z$-axis. The populations $P_\Lambda^{(\kappa)}(t)$ of the $^1D$ substates are monitored. If the populations of the different substates in this frame do not change significantly during the collision, we are dealing with so-called "orbital following".[26,29,40] In the third representation we examine the populations $N_N^{(\kappa)}(t)$ of the five adiabatic states, labeled by $N$, of the Ca + $CH_3X$ system. These adiabatic states are obtained by diagonalizing the 5 × 5 interaction matrix.

When the two particles collide, reaction is assumed to occur through a harpooning mechanism. In other words, if an atom hits the reactive part of the molecule, an electron jumps from Ca to $CH_3X$ at a certain distance $R_h$, forming $Ca^+$ and $CH_3X^-$. This distance $R_h$ is called the harpooning distance. The $Ca^+$ and $CH_3X^-$ particles will then react to form the products CaX ($A^2\Pi$, $B^2\Sigma^+$, $A'^2\Delta$) and $CH_3$ without forming an intermediate reaction complex. The reactive part of the molecule is modeled by a modified version of the angle dependent line of centers (ADLC) model.[23−25,41−44] In this model the molecule is surrounded by an imaginary sphere. Part of this sphere is considered reactive and part is considered nonreactive. The boundary between these two parts is given by the so-called cutoff angle $\beta_c$, which defines the "cone of acceptance". If the angle between the symmetry axis of the $CH_3X$ molecule and the point where the atom hits the sphere, $\beta_R$, is smaller than the cutoff angle, the trajectory is considered reactive. If $\beta_R$ is larger than $\beta_c$, the trajectory is nonreactive. A reactive trajectory (collision) can lead to three different reaction products, CaX ($A^2\Pi$), CaX ($B^2\Sigma^+$), or CaX ($A'^2\Delta$). In the case of Ca + $CH_3F$ and Ca + $CH_3Br$, the $A^2\Pi$ exit channel was measured. The $B^2\Sigma^+$ exit channel could not be measured due to experimental difficulties. For $CH_3Cl$ only the $B^2\Sigma^+$ exit channel was measured. The $A'^2\Delta$ exit channel was not measured in any of the experiments, because it is a metastable species, which lives too long to be detected in the setup used. The three exit channels are labeled by the projection, $\Lambda_f$, of the electronic angular momentum on the CaX axis ($B^2\Sigma^+ \rightarrow \Lambda_f = 0$, $A^2\Pi \rightarrow \Lambda_f = 1$, $A'^2\Delta \rightarrow \Lambda_f = 2$). In experiments by Rettner and Zare[28,29] on Ca + HCl and Ca + $Cl_2$ and in experiments by Soep *et al.*,[30,31] it was found that this projection on the symmetry axis of the product is more or less conserved during the reaction. Hence, we assume that this is also the case for the reactions studied in this article. However, since the rotation of the $CH_3X$ molecule is described quantum mechanically, it is much more convenient to use the projection, $\Lambda$, of the electronic angular momentum on the intermolecular axis instead. This approximation is not very severe, since the intermolecular axis makes an angle of at most 10° with the Ca−X axis, when the Ca atom has arrived at the harpooning radius of 6.0 bohr. This model to determine the electronic state of the product molecule from the projection of the electronic angular momentum on the intermolecular axis, proposed by Menzinger in 1988,[26,27] is called by us the "correlated model". To investigate the influence of this model on the cross sections, we also examine the trajectories using a more approximate model. In the "uncorrelated model" the reactive trajectories all proceed to the same reaction product, regardless of the electronic state at the moment of harpooning. This assumption is equivalent to assuming that the branching ratio for the different products is energy independent. In both our models it is implicitly assumed that the harpooning radius is independent of the orientation of the reagents. We feel that this assumption is not severe, since we have shown in paper 2 that a change of the harpooning radius does not affect the energy dependence of the steric effect very much.

The trajectory calculations have to be performed for a number of impact parameters $b$ and five initial electronic states $N_i$ to obtain a reactive cross section $\sigma_{\Lambda f}^{(j_i,k_i,m_i)}(E)$ for a certain exit channel $\Lambda_f$ ($\Sigma$, $\Pi$, or $\Delta$) and a certain initial rotational state ($j_i$, $k_i$, $m_i$). With these cross sections, we examine three different properties as a function of the translational energy: the total reactive cross section for unoriented molecules, $\sigma_{0,\Lambda f}^{(1,1)}(E)$, the steric effect, $\sigma_{1,\Lambda f}^{(1,1)}(E)/\sigma_{0,\Lambda f}^{(1,1)}(E)$, and the alignment effect, $\sigma_{2,\Lambda f}^{(1,1)}(E)/\sigma_{0,\Lambda f}^{(1,1)}(E)$. The total cross section for unoriented molecules is measured directly in the experiment. In the calculations it is the average of the cross sections for the different $m$-states. Hence, for an exit channel $\Lambda_f$ the total cross section for unoriented molecules initially in a ($j_i$, $k_i$) = (1, 1) rotational state, $\sigma_{0,\Lambda f}^{(1,1)}(E)$, is given by

$$\sigma_{0,\Lambda f}^{(1,1)}(E) = \frac{1}{3}\sum_{m_i=-1}^{1} \sigma_{\Lambda f}^{(1,1,m_i)}(E) \tag{1}$$

For an exit channel $\Lambda_f$ the steric effect $\sigma_{1,\Lambda f}^{(1,1)}(E)/\sigma_{0,\Lambda f}^{(1,1)}(E)$ is calculated as

$$\frac{\sigma_{1,\Lambda f}^{(1,1)}(E)}{\sigma_{0,\Lambda f}^{(1,1)}(E)} = \frac{\sigma_{\Lambda f}^{(1,1,1)}(E) - \sigma_{\Lambda f}^{(1,1,-1)}(E)}{\sigma_{0,\Lambda f}^{(1,1)}(E)} \tag{2}$$

and the alignment effect $\sigma_{2,\Lambda f}^{(1,1)}(E)/\sigma_{0,\Lambda f}^{(1,1)}(E)$ as

$$\frac{\sigma_{2,\Lambda f}^{(1,1)}(E)}{\sigma_{0,\Lambda f}^{(1,1)}(E)} = 5\left[\frac{\sigma_{\Lambda f}^{(1,1,1)}(E) + \sigma_{\Lambda f}^{(1,1,-1)}(E)}{\sigma_0^{(1,1)}(E)} - 2\right] \tag{3}$$

In the uncorrelated model the total reactive cross section for unoriented molecules, $\sigma_0^{(1,1)}(E)$, the steric effect, $\sigma_1^{(1,1)}(E)/\sigma_0^{(1,1)}(E)$, and the alignment effect, $\sigma_2^{(1,1)}(E)/\sigma_0^{(1,1)}(E)$, are calculated using the same formulas as in the correlated model but without the exit channel specification $\Lambda_f$.

Since we only discuss experiments with molecules initially in the ($j_i$, $k_i$) = (1, 1) state, we drop the (1, 1) label from now on.

## III. Computational Details

To perform the calculations the same program was used as in paper 3. It uses a variable order, variable step Adams-Gear

**TABLE 1: Experimental Values of $\sigma_0$ and $\sigma_1(E)/\sigma_0(E)$ for $CH_3Cl$ at Different Energies**

| $E$, (eV) | $\sigma_0(E)$ | $\sigma_1(E)/\sigma_0(E)$ | $E$, (eV) | $\sigma_0(E)$ | $\sigma_1(E)/\sigma_0(E)$ |
|---|---|---|---|---|---|
| 0.177 | 1.44 | −0.17 | 0.319[a] | 1.00 | −0.26 |
| 0.194 | 1.33 | −0.16 | 0.352 | 0.91 | −0.11 |
| 0.214 | 1.45 | −0.18 | 0.395 | 1.02 | −0.14 |

[a] Reference point.

**TABLE 2: Experimental Values of $\sigma_1(E)/\sigma_0(E)$ for $CH_3Br$ at Different Energies**

| $E$ (eV) | $\sigma_1(E)/\sigma_0(E)$ | $E$ (eV) | $\sigma_1(E)/\sigma_0(E)$ |
|---|---|---|---|
| 0.319 | 0.11 | 0.352 | 0.17 |

**TABLE 3: Permanent Multipole Moments for the $CH_3Cl$ Molecule in Atomic Units**

| $l_a$ | $m_a$ | SCF | MP2 | total | literature |
|---|---|---|---|---|---|
| 1 | 0 | −0.8319 | 0.0670 | −0.7649 | 0.746 103 ± 0.000 090[a] |
| 2 | 0 | 1.5357 | −0.0146 | 1.5503 | 0.91 ± 0.6[b] |
| 3 | 0 | 6.4888 | 0.0897 | 6.5785 | |
| 3 | 3 | 3.6882 | 0.0561 | 3.7443 | |

[a] Experimental value. See ref 50. Conversion factor: 1 au = 2.541 58 D. [b] Experimental value. See ref 51.

**TABLE 4: Permanent Multipole Moments for the $CH_3Br$ Molecule in Atomic Units**

| $l_a$ | $m_a$ | SCF | MP2 | total | literature |
|---|---|---|---|---|---|
| 1 | 0 | −0.8369 | 0.1048 | −0.7321 | 0.716 747 ± 0.000 327[a] |
| 2 | 0 | 2.7399 | −0.1342 | 2.8741 | 2.64 ± 0.6[b] |
| 3 | 0 | 5.3978 | 0.3313 | 5.7291 | |
| 3 | 3 | 4.2834 | 0.0467 | 4.3301 | |

[a] Experimental value. See ref 52. Conversion factor: 1 au = 2.541 58 D. [b] Experimental value. See ref 51.

integrator from the NAG-library[45] to propagate the trajectories (subroutine "D02CJF"). The tolerance for the propagation was set to $10^{-6}$. This means that the energy and the norm of the wave function are conserved up to four to six significant figures.

The results for $CH_3F$ are taken from paper 3. For $CH_3Cl$ and $CH_3Br$ calculations were performed at six and two translational energies, respectively. These energies coincided with the experimental energies used by Janssen *et al.*[22] The experimental values for $\sigma_0(E)$ and $\sigma_1(E)/\sigma_0(E)$ for $CH_3Cl$ are given in Table 1. The experimental values for $\sigma_1(E)/\sigma_0(E)$ for $CH_3Br$ are given in Table 2. For $CH_3Br$ no values for $\sigma_0(E)$ were measured.

We have calculated the multipole moments for $CH_3Cl$ and $CH_3Br$ up to the octupole moment at the self-consistent field (SCF) level as well as at the level of second-order Møller−Plesset perturbation theory (MP2), using the ATMOL program package.[46] The (experimental) geometries for $CH_3Cl$ and $CH_3Br$ were taken from refs 47 and 48, respectively. The basis sets for C and H are given in paper 2. The basis sets for Cl and Br were taken from ref 49. The results for $CH_3Cl$ and $CH_3Br$ are given in Tables 3 and 4, respectively. As is clear from these tables the calculated dipole moments are slightly larger than the measured dipole moments. The calculated quadrupole moment of $CH_3Cl$ is also too large compared to experiment. On the other hand, the calculated quadrupole moment of $CH_3Br$ falls within the experimental error bars. For the octupole moments no experimental data were found.

For each translational energy, each electronic state $N_i$ of the Ca atom, and each $m_i$ state, calculations were performed with 17 different impact parameters. These were equally distributed between 0 and 9.0 bohr, in such a way as to enable integration over $b$ with the trapezoidal rule. The rotational constants used in the trajectory calculations were calculated from the geometries

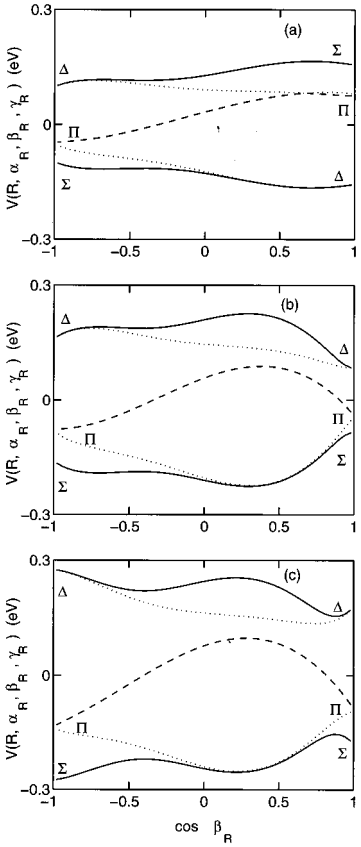


**Figure 1.** Adiabatic PESs as function of cos $\beta_R$ at $R = 6.0$ bohr, $\alpha_R = 0$, and $\gamma_R = 0$. Panel a, Ca + $CH_3F$; panel b, Ca + $CH_3Cl$; panel c, Ca + $CH_3Br$.

used in the electronic structure calculations. The maximum impact parameter of 9.0 bohr turned out to be large enough not to miss any reactive trajectories. Each trajectory started at $R = 30$ bohr. The harpooning radius was taken to be 6.0 bohr for both $CH_3Cl$ and $CH_3Br$. Three cutoff angles $\beta_c = 90°$, 120°, and 180° were used to determine the influence of the cutoff angle on the steric effect and on its energy dependence. Therefore, the calculations will be called "model 90", "model 120", and "model 180" calculations, respectively.

For the calculations we used an IBM RS/6000 390 workstation. Trajectories typically took 70 min. For each trajectory the number of coupled equations was 198 558, the number of function evaluations was on the order of 300, and the memory use was on the order of 210 Mb.

## IV. Results and Discussion

The SC results using the correlated model for the CaX ($B^2\Sigma^+$, $A^2\Pi$, $A'^2\Delta$) exit channels will be designated by SC-Σ, SC-Π, and SC-Δ, respectively. The SC results using the uncorrelated model for the Ca + $CH_3X$ reaction are designated by SC. First, we discuss the potentials of the three systems, trapping, reorientation, and the evolution of the electronic state of Ca. Then we turn to the discussion of the cross sections.

**A. The Interaction Potentials.** The multipole moments used to construct the PESs are in Tables 3 and 4 for $CH_3Cl$ and $CH_3Br$, respectively. The multipole moments for $CH_3F$ are taken from paper 2. The adiabatic PESs for the Ca + $CH_3F$, Ca + $CH_3Cl$, and Ca + $CH_3Br$ systems are given in Figure 1 as a function of cos $\beta_R$ at $R = 6.0$ bohr, $\alpha_R = 0°$, and $\gamma_R = 0°$. The labels Σ, Π, and Δ on the PESs are the symmetry character of the corresponding adiabatic eigenstates around $\beta_R = 0$ and $\beta_R = \pi$, where the eigenstates are pure states. The three panels

**TABLE 5: Trapping Data. Every Second Impact Parameter is Left Out**

| $x_i$ | $x_f$ ($CH_3F$) | $z_f$ ($CH_3F$) | $x_f$ ($CH_3Cl$) | $z_f$ ($CH_3Cl$) |
|---|---|---|---|---|
| 0.0 | 0.0 | 6.0 | 0.0 | 6.0 |
| 3.2 | 3.0 | 5.2 | 3.0 | 5.2 |
| 4.5 | 4.2 | 4.3 | 4.3 | 4.2 |
| 5.5 | 5.1 | 3.1 | 5.1 | 3.0 |
| 6.4 | 5.8 | 1.6 | 5.8 | 1.5 |
| 7.1 | 5.9 | −1.0 | 5.9 | −1.2 |

in this figure show that the potentials for these systems are on the same order of magnitude (between −0.3 and 0.3 eV). The most remarkable difference is that the order of the Σ, Π, Δ character of the PESs of the Ca + $CH_3Cl$ and Ca + $CH_3Br$ systems around $\beta_R = 0$ is reversed with respect to the Ca + $CH_3F$ system. The reason for this difference between Ca + $CH_3F$ on the one hand and Ca + $CH_3Cl$ and Ca + $CH_3Br$ on the other hand lies in the fact that the quadrupole moments of $CH_3Cl$ and $CH_3Br$ are substantially larger than the quadrupole moment of $CH_3F$ and have a different sign. The difference in the Σ, Π, Δ character might seem large at first. However, if one inspects the dominant symmetry character of the eigenvectors belonging to a certain PES, defined by the sum over squares of the coefficients of the basisfunctions of a certain symmetry, between cos $\beta_R = 1$ and cos $\beta_R = -1$, it turns out that only between cos $\beta_R = 1$ and cos $\beta_R = 0.9$ the symmetry assignments between the three panels are different. Between cos $\beta_R = -1$ and cos $\beta_R = 0.9$ they are the same.

**B. Trapping and Reorientation.** We wish to examine the role of trapping and reorientation during the approach of the two colliding particles. From previous work[23−25] we know that both phenomena are important, especially at low energies on the attractive PESs. Furthermore, we know that the effects of trapping and reorientation on the reactive cross sections cancel each other to some extent. We will examine these phenomena for Ca + $CH_3F$ and Ca + $CH_3Cl$ at the experimental energies $E = 0.182$ eV and $E = 0.177$ eV, respectively. For Ca + $CH_3$-Br trapping and reorientation are not expected to be very important, because this reaction was only measured at relatively high translational energies. Therefore, we focus on Ca + $CH_3F$ and Ca + $CH_3Cl$ and examine trapping for trajectories on the most attractive PES ($N_i = 1$), starting in a $m_i = 1$ state (i.e., the projection of $j$ on the space-fixed $z$-axis equals 1).

A measure of the degree of trapping are the $x$- and $z$-coordinates of the atom with respect to the molecule in the space fixed frame during the collision. If there is no trapping, then $z$ is always positive (the atom approaches from the $+z$-direction in all cases). Furthermore, in case of negligible trapping the $x$-coordinate will not change (straight-line trajectory). The $y$-coordinate is not very important, since the trajectories start in the $xz$-plane ($y = 0$) and the deviation from this plane appears to be negligible. In Table 5 we give the initial coordinate $x_i$ of the atom with respect to the molecule for both reactions in column 1 ($z_i$ is approximately 30.0 in all cases). In columns 2 and 3 we give the coordinates ($x_f$, $z_f$) at the harpooning radius, $R = 6.0$ bohr, for the Ca + $CH_3F$ reaction and in column 4 and 5 the coordinates ($x_f$, $z_f$) at $R = 6.0$ bohr for the Ca + $CH_3Cl$ reaction. We have omitted every second reactive impact parameter to obtain a more clear presentation. From this table it is clear that there is a considerable amount of trapping for both systems, especially for the trajectories with large impact parameters (large $x_i$). There is not much difference between Ca + $CH_3F$ and Ca + $CH_3Cl$. Apparently, the influence of the larger reduced mass (≈20%) of the Ca + $CH_3Cl$ system is not visible at this energy.

For both systems also a large amount of reorientation is found. We plotted the final probability function for the direction of the C−X axis in the SF frame (given by polar angle $\beta$ and azimuthal angle α) for the Ca + $CH_3F$ reaction at $b = 3.89$, 5.95, and 7.11 bohr in Figure 2. For Ca + $CH_3Cl$ the ($\beta$, α) probability functions at the same impact parameters are plotted in Figure 3. In all cases the initial ($\beta$, α) probability distribution function corresponds to the ($j$, $k$, $m$) = (1, 1, 1) state and is given by Figure 10, panel a in paper 3. The position of the atom is indicated in each panel by the arrow. From these figures it is clear that, for both systems, there is not only reorientation in the $\beta$-angle, but also in the α-angle. However, the two systems show remarkable differences for this phenomenon. For Ca + $CH_3F$ we see first a localization of the wave function around α = 0 and then a reorientation of this localized wave function to follow the atom in its motion around the molecule. For Ca + $CH_3Cl$ we see that the wave function "splits", in the α-angle and that it spreads in the $\beta$-angle. The difference between Ca + $CH_3F$ and Ca + $CH_3Cl$ can be understood from differences in the PESs, plotted as a function of $\beta$ and α. We plotted these PESs for a number of values of the coordinates and this shows that the wave function follows the potential. From this observation we conclude that the $CH_3F$ and $CH_3Cl$ molecules behave more or less like classical particles with respect to rotation. Quantum effects do not seem to be very important, except for generating the correct initial state distribution.

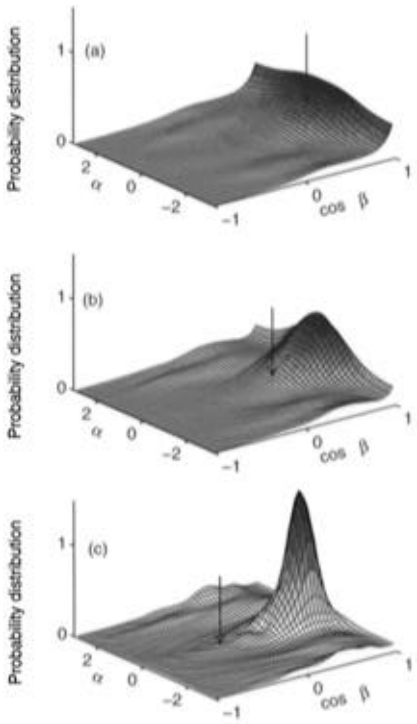


**Figure 2.** Final probability distribution at $R = 6.0$ bohr for the direction of the C−F axis as a function of the polar angle $\beta$ and the azimuthal angle α at $b = 3.89$ bohr (panel a), $b = 5.95$ bohr (panel b), and $b = 7.11$ bohr (panel c). Initial conditions: $E = 0.182$ eV, $m_i = 1$, and $N_i = 1$. Arrow designates position of atom. Panel a: ($x_f$, $z_f$) = (3.7, 4.7). Panel b: ($x_f$, $z_f$) = (5.5, 2.5). Panel c: ($x_f$, $z_f$) = (5.9, −1.0).

**C. Evolution of the Electronic State of Ca.** As explained in section II we have chosen three representations in which to examine the evolution of the electronic states of Ca. Again, we focus primarily on the difference between Ca + $CH_3F$ and Ca + $CH_3Cl$. Since the character of the electronic states depends on the initial conditions, we have chosen a few characteristic examples. The impact parameter is in all cases 6.0 bohr. The initial rotational state ($j_i$, $k_i$, $m_i$) is in all cases (1, 1, 1).

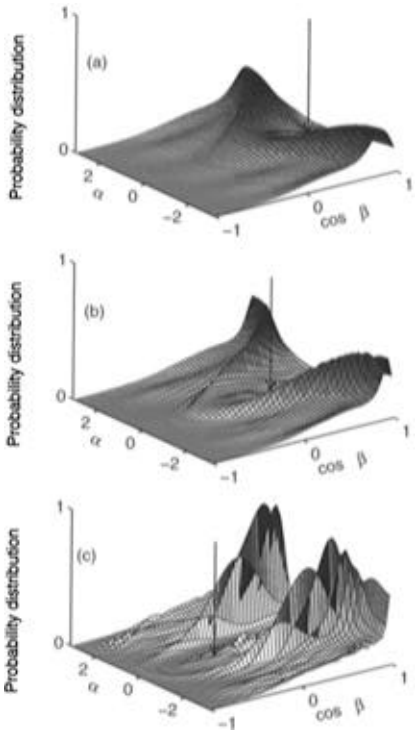


**Figure 3.** Final probability distribution at $R = 6.0$ bohr for the direction of the C−Cl axis as a function of the polar angle $\beta$ and the azimuthal angle $\alpha$ at $b = 3.89$ bohr (panel a), $b = 5.95$ bohr (panel b), and $b = 7.11$ bohr (panel c). Initial conditions: $E = 0.177$ eV, $m_i = 1$, and $N_i = 1$. Arrow designates position of atom. Panel a: $(x_f, z_f) = (3.7, 4.7)$. Panel b: $(x_f, z_f) = (5.5, 2.4)$. Panel c: $(x_f, z_f) = (5.9, -1.2)$.

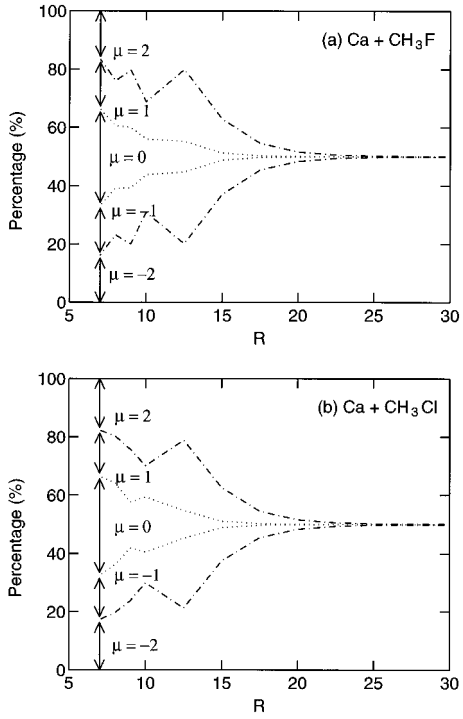


**Figure 4.** Cumulative population of the $^1D$ substates of Ca in the SF frame for $b = 6.0$ bohr, $m_i = 1$, and $N_i = 1$. Panel a: Ca + $CH_3F$ at $E = 0.182$ eV. Panel b: Ca + $CH_3Cl$ at $E = 0.177$ eV.

In Figure 4 we have plotted the populations $Q_\mu^{(\kappa)}(t)$ of the substates $\mu$ of the $^1D$ state of Ca with respect to the SF frame. The results for the Ca + $CH_3F$ and Ca + $CH_3Cl$ reactions are shown in panels a and b, respectively. Figure 4 is a cumulative plot, i.e., the area between two lines is the population of a certain state, as is indicated by the double headed arrow. In both cases

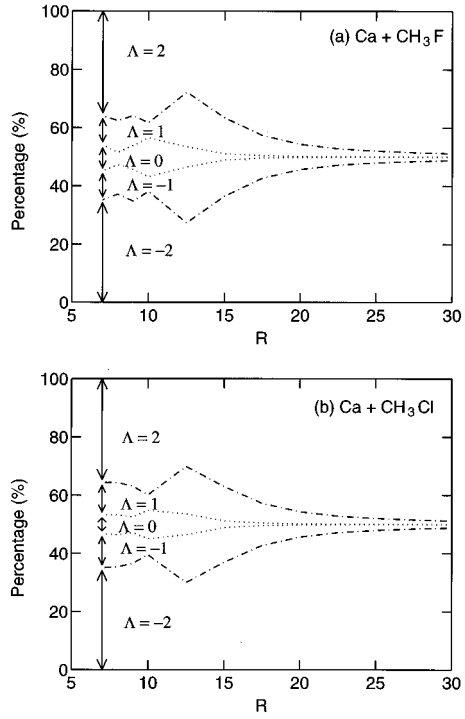


**Figure 5.** Cumulative population of the $^1D$ substates of Ca in the DF frame for $b = 6.0$ bohr, $m_i = 1$, $E = 0.119$ eV, and $N_i = 1$. Panel a: Ca + $CH_3F$ at $E = 0.182$ eV. Panel b: Ca + $CH_3Cl$ at $E = 0.177$ eV.

the trajectory was started on the most attractive initial PES ($N_i = 1$), which corresponds to a linear combination of the $\mu = 2$ and $\mu = -2$ states. From Figure 4 it is clear that the evolution of the Ca electronic state is far from diabatic, because in that case the populations would have been constant. The scrambling of the $\mu$-states starts already at large separations ($R \approx 25$ bohr) for both Ca + $CH_3F$ and Ca + $CH_3Cl$. At shorter distances it seems that the wave function becomes prepared in a $\mu = 0$ state. Inspection of the eigenvectors for the potential around the harpooning radius shows that at this moment the wave function is in an area of the potential where the most important eigenvectors have predominantly $\Sigma$ character. Apparently, at this translational energy the wave function adapts itself almost instantaneously to the potential. At higher energies, this will no longer be true and the populations of the $^1D$ substates will resemble more the initial situation. It is interesting to note that the scrambling of $\mu$ is a very efficient process. One has to increase the translational energy to approximately 1000 eV to quench it completely.

In Figure 5 we examine the populations $P_\Lambda^{(\kappa)}(t)$ of the $^1D$ substates $\Lambda$ in the DF frame in which the intermolecular axis is the $z$-axis. Again, the trajectory is started in the $N_i = 1$ initial state, which in this frame corresponds to an almost pure $\Lambda = \pm 2$ state ($= \Delta$ symmetry). If the populations do not change, we may say there is "orbital following".[26,29,40] As is clear from Figure 5 this is not entirely the case, since the populations do change during the approach. It is clear, however, that $\Lambda$ is better conserved than $\mu$. The differences between Ca + $CH_3F$ in panel a and Ca + $CH_3Cl$ in panel b are again minor. If we compare the Ca + $CH_3F$ results in panel a to the results in paper 3, we see that the scrambling starts a little later, but that the amount of scrambling is comparable. Apparently, the fact that the energy for panel a is approximately 1.5 times higher than the energy used in paper 3 is not very influential for the amount of scrambling.

In Figure 6 we examine the populations of the eigenstates $N$ of the interaction matrix, as defined in paper 3, eq 30. The

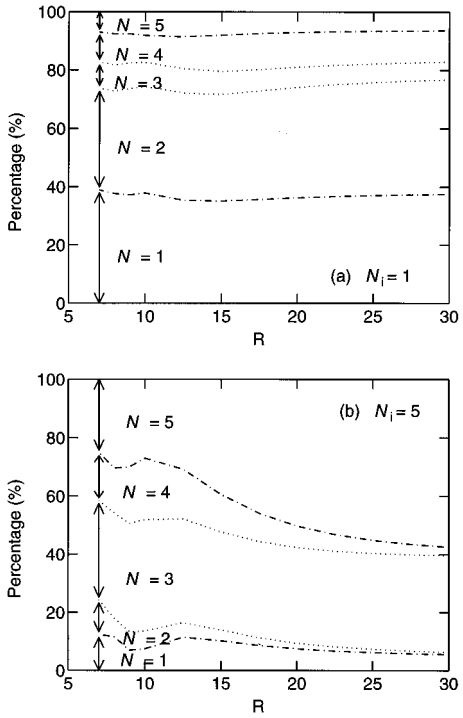


**Figure 6.** Cumulative population of the eigenstates of the interaction matrix for Ca + $CH_3Cl$ in the DF frame for $b = 6.0$ bohr, $m_i = 1$, and $E = 0.177$ eV. Panel a: Ca + $CH_3Cl$ for $N_i = 1$. Panel b: Ca + $CH_3Cl$ for $N_i = 5$.

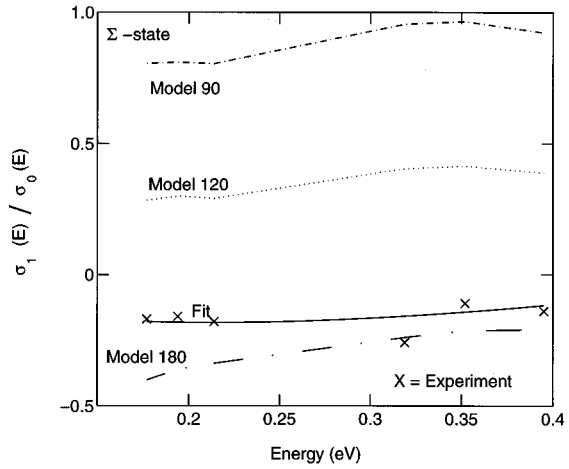


**Figure 7.** SC results for $\sigma_1(E)/\sigma_0(E)$ for Ca + $CH_3Cl \rightarrow CaCl(B^2\Sigma^+)$ + $CH_3$ for different cutoff angles (with the correlation model). Also the experimental data and a fit to the experimental data are plotted.

**TABLE 6: Steric Effect for the Ca + $CH_3Br \rightarrow CaBr(A^2\Pi)$ + $CH_3$ Reaction for Different Translational Energies and Different Cutoff Angles Using the Uncorrelated Model and the Correlated Model**

| | uncorrelated model | | correlated model | |
|---|---|---|---|---|
| | 0.319 eV | 0.352 eV | 0.319 eV | 0.352 eV |
| model 90 | 0.92 | 0.96 | 0.84 | 0.89 |
| model 120 | 0.49 | 0.52 | 0.40 | 0.43 |
| model 180 | 0.00 | 0.03 | −0.15 | −0.12 |

results for Ca + $CH_3F$ do not differ much from the results in paper 3. Therefore, they are not given here. Figure 6, panels a and b, shows clearly that $N_i$ and $N$ are not the same (see section II). In fact, the calculation is started in a pure $N_i$ state, but in a mixture of adiabatic states $N$. For a trajectory starting in the $N_i = 1$ state (Figure 6, panel a) the populations of the adiabatic states $N$ for Ca + $CH_3Cl$ do not change much during the approach of the colliding particles. This means that the adiabatic description fits the evolution of the Ca $^1D$ states very well, as was the case for Ca + $CH_3F$. Only at relatively short distances is there a substantial deviation from pure adiabatic behavior. It seems that the Ca + $CH_3Cl$ curves in panel (a) are flatter than those for Ca + $CH_3F$ in paper 3. This suggests that the evolution of the electronic state of Ca in the case of Ca + $CH_3Cl$ is slightly more adiabatic than in the case of Ca + $CH_3F$. The reason for this small difference is not clear.

For the $N_i = 5$ initial state, which corresponds to the most repulsive initial PES, the amount of nonadiabatic behavior is considerably larger (see Figure 6, panel b) than for the $N_i = 1$ initial state. The population of the lowest lying electronic states increases during the collision, whereas the population of the $N = 3$ and $N = 5$ states decreases. That is, electronic energy is released during the collision.

Concluding, we can say that for Ca + $CH_3F$ and Ca + $CH_3Cl$ the evolution of the Ca electronic state is largely adiabatic for the $N_i = 1$ initial state. For the higher initial states ($N_i > 1$) nonadiabatic effects become more important.

**D. The Steric Effect.** The experimental results for Ca + $CH_3Cl \rightarrow CaCl(B^2\Sigma^+)$ + $CH_3$ show a *negative* steric effect, which is relatively independent of the translational energy. Using the uncorrelated model this cannot be explained, because for this model the lowest steric effect is zero (model 180 calculation). With the correlated model it is possible to obtain a negative steric effect, as was shown in paper 3. The SC-Σ results are shown in Figure 7. A cutoff angle of about 150° would give the best agreement with experiment. This angle is larger than the cutoff angle $\beta_c$ that we find for the Ca + $CH_3F$ reaction ($\beta_c = 105°$). This correlates well with the fact that chlorine is larger than fluorine (e.g., if one compares the van der Waals radii of both atoms).

For Ca + $CH_3Br \rightarrow CaBr(A^2\Pi)$ + $CH_3$ the results for the uncorrelated and the correlated model are in Table 6. For SC-Π we see that the steric effect drops by approximately 0.1 for a given cutoff angle with respect to the SC-Br calculations. In the uncorrelated model a cutoff angle of 155° reproduces the experiment and in the correlated model a cutoff angle of 140°. Beforehand, we expected to find a larger cutoff angle than the angle of 150°, found for Ca + $CH_3Cl$, because bromine is larger than chlorine. However, only two data points were measured for Ca + $CH_3Br$, making it impossible to estimate the accuracy of the experimental points. This makes the cutoff angle for Ca + $CH_3Br$ less accurate than the cutoff angle for Ca + $CH_3F$ or Ca + $CH_3Cl$, which might explain the discrepancy.

If we compare the curves for $CH_3F$, $CH_3Cl$, and $CH_3Br$ for each of the three exit channels in Figure 8, we see that, for a given exit channel and cutoff angle, they are remarkably similar. Apparently, the differences in the PESs cancel to a large extent in the calculation of the cross sections. If we compare the curves for the Σ exit channel to the curves for the Π exit channel for a given cutoff angle and reactive system, we see small differences between the curves. The curves for the Δ exit channel are entirely different.

In the discussion of the steric effect for the Ca + $CH_3F$ reaction in paper 3, we used a qualitative reasoning based on the symmetry assignments of the PESs around $\cos \beta_R = -1$ and $\cos \beta_R = 1$ to understand sign and energy dependence of the steric effect. For Ca + $CH_3Cl$ and Ca + $CH_3Br$ this "model" becomes more elaborate, because of the rapid changes in dominant symmetry around $\cos \beta_R = 1$. However, we feel that it can still explain the energy dependence of the steric effect and its magnitude as a function of cutoff angle. We first discuss the consequences of the model for the Σ exit channel, a cutoff angle $\beta_c = 180°$, and a low translational energy (see Figure 8,

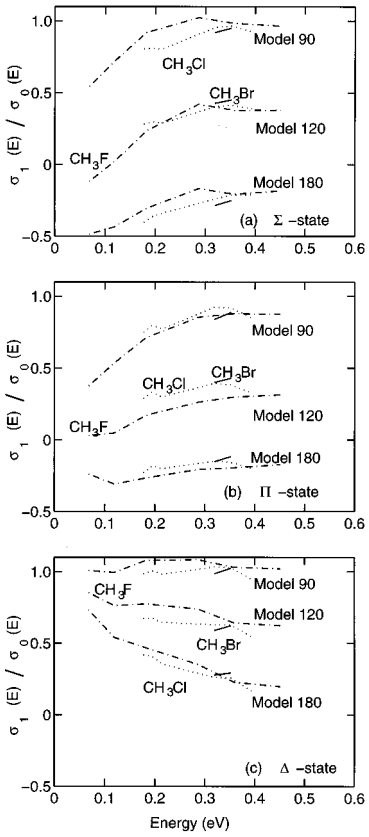


**Figure 8.** SC results for $\sigma_1(E)/\sigma_0(E)$ for Ca + $CH_3X$ (X = F, Cl, Br) → CaX + $CH_3$ for different cutoff angles (with the correlation model). Solid curves, Ca + $CH_3Br$; dashed curves, Ca + $CH_3F$; and dotted curves, Ca + $CH_3Cl$. Panel a: $B^2\Sigma^+$ exit channel. Panel b: $A^2\Pi$ exit channel. Panel c: $A'^2\Delta$ exit channel.

panel a). From this starting point the effects for other cutoff angles and energies and for the other exit channels can be inferred. With a cutoff angle of 180°, one samples all values of $\beta_R$. For the unfavorable reaction geometry ($m_i = -1$) the final orientational probability distribution shows a maximum around $\beta_R = \pi$, where the lowest potential energy surface has a Σ character (see Figure 1, panels b and c). Therefore, the cross section for the reaction to the $B^2\Sigma^+$ exit channel for this reaction geometry, $\sigma_\Sigma^{(1,1,-1)}$, is large. For the favorable reaction geometry ($m_i = 1$) the final orientational probability distribution shows a maximum around $\beta_R = \pi/3$. This implies that the systems proceed mainly to the $A'^2\Delta$ exit channel, because the dominant symmetry character of the eigenstates associated with the lowest two PESs (on which most of the reactive trajectories are) is Δ. Therefore, it seems plausible that the cross section for the reaction to the $B^2\Sigma^+$ exit channel for the favorable reaction geometry, $\sigma_\Sigma^{(1,1,1)}$, is smaller than $\sigma_\Sigma^{(1,1,-1)}$, which results in a negative steric effect for a model 180 calculation. Decreasing the cutoff angle excludes the region around $\beta_R = \pi$ and affects $\sigma_\Sigma^{(1,1,-1)}$ more than $\sigma_\Sigma^{(1,1,1)}$. Therefore, for smaller cutoff angles the steric effect increases and becomes positive. Increasing the energy causes a drop in $\sigma_\Sigma^{(1,1,-1)}$, because more trajectories end up on higher PESs (whose eigenstates have a different Σ, Π, Δ character). For the same reason $\sigma_\Sigma^{(1,1,1)}$ increases slightly. This means that the steric effect increases with increasing energy. One can apply the same model for the $A^2\Pi$ and $A'^2\Delta$ exit channels and explain the size and energy dependence of the steric effect for different cutoff angles and different translational energies, for each exit channel, which are plotted in Figure 8, panels b and c.

Summarizing, it can be said that there are two reasons for the differences in the measured steric effect between the Ca + $CH_3F$ and Ca + $CH_3Cl$ reactions. First, there is the effect of the larger cutoff angle in case of Ca + $CH_3Cl$. Second, there is the effect from the fact that for Ca + $CH_3Cl$ a different exit channel was measured. From the results in Figure 8 it follows that the effect of the larger cutoff angle is much more important than the effect from the different exit channel. This might seem contradictory to the experimental results, where a *positive* steric effect was found for the $A^2\Pi$ exit channel of Ca + $CH_3F$ and Ca + $CH_3Br$ and a *negative* steric effect for the $B^2\Sigma^+$ exit channel of Ca + $CH_3Cl$. However, we also predict a *negative* steric effect for the $A^2\Pi$ exit channel of Ca + $CH_3Cl$ of approximately −0.05, relatively independent of the translational energy. This channel was not measured for this reaction, however. For Ca + $CH_3Br$ the experimental data are scarce. Although the measured steric effect is positive in this case, it is small and closer to the result for Ca + $CH_3Cl$ than to the result for Ca + $CH_3F$. This supports our conclusion. Long-range effects are important to obtain the correct energy dependence of the steric effect, as found for the Ca + $CH_3F$ system. However, the differences in the steric effect for the three systems are dominated by the effect of different cutoff angles, rather than by differences in the long-range potentials.

**E. The Total Cross Section and Branching Ratios.** For Ca + $CH_3Cl$ neither the SC nor the SC-Σ results reproduce the experimental energy dependence of the total reactive cross section for unoriented molecules very well. This is not entirely unexpected, since for Ca + $CH_3F$ → CaF ($A^2\Pi$) + $CH_3$ the experimental $\sigma_0(E)$ was not reproduced either. In paper 3 we gave two possible reasons for this failure to reproduce the experimental results. Either important elements are missing from the potential, such as induction or dispersion, or the description of the harpooning mechanism is not accurate enough. Also, harpooning may take place at a separation of approximately 10 bohr (at the so-called outer crossing), leading to ground state products.[22,24] This harpooning may be both energy and orientation dependent and affect indirectly the measured cross sections. However, we are not able to quantify this effect, since the reaction to the ground state was not examined experimentally.

The SC-Br results and the SC-Br-Π results for $\sigma_0(E)$ are all, within a few percent, energy independent. The total cross section for unoriented molecules was not measured for this system. However, we think that, in view of the results for Ca + $CH_3F$ and Ca + $CH_3Cl$, the results for Ca + $CH_3Br$ will not reproduce the experiment either. However, if we assume that comparable errors are made for all $\sigma_0(E)$, the branching ratios for the different exit channels will still be meaningful.

The branching ratios $\sigma_{0,\Sigma}(E)/\sigma_{0,\Pi}(E)$ between the $B^2\Sigma^+$ and $A^2\Pi$ exit channels for the three Ca + $CH_3X$ reactions are given in Table 7 together with the experimental values. The experimental values were all obtained from experiments with a $CH_3X$ gas cell instead of a beam. We have given the calculated branching ratios at low energy ($E = 0.182$ eV for Ca + $CH_3F$, $E = 0.177$ eV for Ca + $CH_3Cl$) and at high energy ($E = 0.358$ eV for Ca + $CH_3F$, $E = 0.352$ eV for Ca + $CH_3Cl$ and Ca + $CH_3Br$). For the calculated branching ratios we have taken the cutoff angle which gave the best results in the calculation of the steric effect, i.e., 105° for Ca + $CH_3F$, 150° for Ca + $CH_3Cl$, and 140° for Ca + $CH_3Br$. The branching ratios turn out to be relatively independent of the translational energy. They show a decreasing trend in going from $CH_3F$ to $CH_3Br$. However, the correspondence between theory and experiment is only qualitative.

**TABLE 7: Branching Ratio $[\sigma_{0,\Sigma}(E)/\sigma_{0,\Pi}(E)]$ between the $B^2\Sigma^+$ and the $A^2\Pi$ Exit Channels and Branching Ratio $[\sigma_{0,\Delta}(E)/\sigma_{0,\Pi}(E)]$ between the $A'^2\Delta$ and the $A^2\Pi$ Exit Channels for the Ca + $CH_3F$, Ca + $CH_3Cl$, and Ca + $CH_3Br$ Reactions. Also the Experimental Values for $[\sigma_{0,\Sigma}(E)/\sigma_{0,\Pi}(E)]$ Are Given**

| | $\sigma_{0,\Sigma}(E)/\sigma_{0,\Pi}(E)$ | | | $\sigma_{0,\Delta}(E)/\sigma_{0,\Pi}(E)$ | |
|---|---|---|---|---|---|
| reaction | "low" energy[a] | "high" energy[b] | exptl | "low" energy | "high" energy |
| Ca + $CH_3F$ | 0.45 | 0.49 | 1−5.6[c] | 1.6 | 1.3 |
| Ca + $CH_3Cl$ | 0.42 | 0.45 | 0.67[d] | 1.1 | 1.1 |
| Ca + $CH_3Br$ | *e* | 0.43 | 0.2−0.3[f] | *e* | 1.1 |

[a] $E = 0.182$ eV for Ca + $CH_3F$. $E = 0.177$ eV for Ca + $CH_3Cl$. [b] $E = 0.358$ eV for Ca + $CH_3F$. $E = 0.352$ eV for Ca + $CH_3Cl$ and Ca + $CH_3Br$. [c] See ref 14. [d] See ref 53. [e] Not calculated. [f] See ref 54.

The branching ratios $\sigma_{0,\Delta}(E)/\sigma_{0,\Pi}(E)$ between the $A'^2\Delta$ and $A^2\Pi$ exit channels for the three Ca + $CH_3X$ reactions are given in Table 7 for the same two energies as the $\sigma_{0,\Sigma}(E)/\sigma_{0,\Pi}(E)$ branching ratios. No experimental values are known for these branching ratios. The $\sigma_{0,\Delta}(E)/\sigma_{0,\Pi}(E)$ branching ratios turn out to be more energy dependent than the $\sigma_{0,\Sigma}(E)/\sigma_{0,\Pi}(E)$ branching ratios for the Ca + $CH_3F$ reaction. They also decrease when going from $CH_3F$ to $CH_3Cl$ but do not change when going from $CH_3Cl$ to $CH_3Br$. However, we think that we can conclude from the $\sigma_{0,\Sigma}(E)/\sigma_{0,\Pi}(E)$ and the $\sigma_{0,\Delta}(E)/\sigma_{0,\Pi}(E)$ branching ratios that the $A^2\Pi$ exit channel becomes more important for heavier methyl halides.

**F. The Alignment Effect.** The alignment effect was not measured experimentally for the Ca + $CH_3Br$ reaction. For the Ca + $CH_3Cl$ reaction it was found to scatter around zero.[22] The calculations show that it is on the order of −0.1 in the case of Ca + $CH_3Cl$, relatively independent of translational energy or exit channel. For the Ca + $CH_3Br$ reaction, the alignment effect is found to be approximately zero, again independently of the translational energy and the exit channel. These findings are consistent with the findings for Ca + $CH_3F$, where a similar result was obtained, both by calculations and by the experiment.

## V. Conclusions

We have performed semiclassical calculations on the Ca ($^1D$) + $CH_3X$ (X = F, Cl, Br) reactive systems. The potential for these systems consists of five asymptotically degenerate PESs. The relative motion of Ca with respect to $CH_3X$ was treated classically; the rotation of the $CH_3X$ molecule and the electronic state of Ca and $CH_3X$ were treated quantum mechanically. Two models were used to describe the reaction probability. The first model, a modified version of the ADLC model, was used to describe the reactive part of the $CH_3X$ molecule; i.e., it was used to determine whether a trajectory was reactive or nonreactive. The second model, to which we refer as the correlated model, was used to describe the reactivity for different exit channels of the reaction. In this model it is assumed that the projection of the electronic angular momentum on the intermolecular axis is conserved during the reaction. This projection becomes the projection of the electronic angular momentum of the product on its symmetry axis.

For the Ca + $CH_3F$ and Ca + $CH_3Cl$ reactions we examined some trajectories in more detail for the occurrence of trapping and reorientation of the incoming molecule. Both reactions show comparable amounts of trapping. With respect to reorientation, these reactions turn out to behave differently. Calculations on Ca + $CH_3F$ show a localization of the probability distribution of the C−F axis toward the incoming atom, although somewhat lagging behind. Calculations on Ca + $CH_3Cl$ show a localization of the C−Cl axis in the azimuthal angle $\alpha$ but a spread in the polar angle $\beta$. The cause for this difference lies in the differences in the PESs as a function of $\beta$ and $\alpha$ for these systems.

The evolution of the electronic state of Ca ($^1D$) in the Ca + $CH_3F$ and Ca + $CH_3Cl$ reactions can be viewed as nearly adiabatic for the most attractive PES. For less attractive and repulsive PESs, nonadiabatic effects start to play a larger role. We also conclude that "orbital following" in terms of "pure" substates of the $^1D$ state occurs to some extent, but cannot completely describe the evolution of the Ca electronic state. The original substates $\mu = -2, ..., 2$ of the $^1D$ state with respect to the laboratory (SF) axes are completely scrambled during the collision.

With the models for the reaction probability, described in the first paragraph, it is possible to reproduce the experimentally measured steric effect for the reactions Ca + $CH_3F \rightarrow$ CaF ($A^2\Pi$) + $CH_3$ (see also ref 25), Ca + $CH_3Cl \rightarrow$ CaCl ($B^2\Sigma^+$) + $CH_3$, and Ca + $CH_3Br \rightarrow$ CaBr ($A^2\Pi$) + $CH_3$. To reproduce the experiment for these three reactions a "cone of acceptance" with cutoff angles of 105°, 150°, and 140° was used, respectively. The increase in the cutoff angle, when going from $CH_3F$ to $CH_3Cl$ and $CH_3Br$, is consistent with the fact that Cl and Br are larger than F. The difference in cutoff angle between Ca + $CH_3Cl$ and Ca + $CH_3Br$ may reflect subtle differences in the (short-range) reaction dynamics, which are not included in our (crude) reaction model. The negative steric effect for the Ca + $CH_3Cl$ reaction, which seemed so surprising at first, is an effect of the large cutoff angle for $CH_3Cl$ rather than an effect of the $B^2\Sigma^+$ exit channel, which was measured for Ca + $CH_3$-Cl. Reexamination of the experimental results shows that this conclusion is not contradicted by the measurements. The long-range potentials used are necessary to obtain the correct energy dependence for the steric effect, as measured for the Ca + $CH_3F$ system. However, for the observed differences in the steric effect, differences in the cutoff angles are more important than differences in the long-range potentials.

The energy dependence of the experimental cross sections for unoriented molecules, $\sigma_0(E)$, cannot be reproduced by our calculations. In general, this energy dependence is too weak compared to experiment for all three reactions studied. The branching ratios $\sigma_{0,\Sigma}(E)/\sigma_{0,\Pi}(E)$ for the three reactions show the same qualitative behavior as the experimentally measured branching ratios, when going from $CH_3F$ to $CH_3Br$. However, there is no quantitative agreement between theory and experiment for this property. There might be two possibilities to obtain more accurate results for $\sigma_0(E)$. First, the modeling of the reaction probability can be improved by using, e.g., Landau-Zener type transition probabilities to model the harpooning event. Second, it is possible to include other Ca or $CH_3X$ electronic states in the calculation, in order to introduce polarization effects and dispersion forces. Also the inclusion of $Ca^+$ and $CH_3X^-$ electronic states might improve the calculation.

In general, we conclude that we have shown that the correlated model is able to reproduce the experimentally measured steric effect for the reactions studied in this article. Furthermore, we have shown that it is possible to make qualitative ideas about these reactive systems more quantitative with the models used in our calculations.

**Acknowledgment.** We thank Dr. Maurice H. M. Janssen for many stimulating discussions and useful comments regarding this work. We also thank Professor Dr. David H. Parker for

reading the manuscript. A.J.H.M.M. thanks the Netherlands Foundation for Chemical Research (SON) and the Netherlands Organization for the Advancement of Research (NWO) for financial support. G.C.G. thanks the Royal Netherlands Academy for the Arts and the Sciences (KNAW) for financial support.

## References and Notes

(1) Kramer, K. H.; Bernstein, R. B. *J. Chem. Phys.* **1965**, *42*, 767.
(2) Chakravorty, K. K.; Parker, D. H.; Bernstein, R. B. *Chem. Phys.* **1982**, *68*, 1.
(3) Beuhler, R. J.; Bernstein, R. B. *J. Chem. Phys.* **1969**, *51*, 5365.
(4) Parker, D. H.; Chakravorty, K. K.; Bernstein, R. B. *J. Phys. Chem.* **1981**, *85*, 466.
(5) Parker, D. H.; Chakravorty, K. K.; Bernstein, R. B. *Chem. Phys. Lett.* **1982**, *86*, 113.
(6) Stolte, S.; Chakravorty, K. K.; Bernstein, R. B.; Parker, D. H. *Chem. Phys.* **1982**, *71*, 353.
(7) Brooks, P. R.; Jones, E. M. *J. Chem. Phys.* **1966**, *45*, 3449.
(8) Marcelin, G.; Brooks, P. R. *J. Am. Chem. Soc.* **1973**, *95*, 7785.
(9) Marcelin, G.; Brooks, P. R. *J. Am. Chem. Soc.* **1975**, *97*, 1710.
(10) Van de Ende, D.; Stolte, S. *Chem. Phys.* **1984**, *89*, 121.
(11) Jalink, H.; Parker, D. H.; Stolte, S. *J. Chem. Phys.* **1986**, *85*, 5372.
(12) Jalink, H. Ph. D. Thesis, KUN Nijmegen NL, 1987.
(13) Janssen, M. H. M. Ph. D. Thesis, KUN Nijmegen NL, 1989.
(14) Janssen, M. H. M.; Parker, D. H.; Stolte, S. *J. Phys. Chem.* **1991**, *95*, 8142.
(15) Loesch, H. J.; Remscheid, A. *J. Chem. Phys.* **1990**, *93*, 4779.
(16) Loesch, H. J.; Stenzel, E.; Wüstenbecker, B. *J. Chem. Phys.* **1991**, *95*, 3841.
(17) Friedrich, R.; Herschbach, D. R. *Nature* **1991**, *353*, 412.
(18) Loesch, H. J.; Möller, J. *J. Chem. Phys.* **1992**, *97*, 9016.
(19) Loesch, H. J.; Stienkemeier, F. *J. Chem. Phys.* **1993**, *98*, 9570.
(20) Loesch, H. J.; Stienkemeier, F. *J. Chem. Phys.* **1994**, *100*, 740.
(21) Loesch, H. J.; Stienkemeier, F. *J. Chem. Phys.* **1994**, *100*, 4308.
(22) Janssen, M. H. M.; Parker, D. H.; Stolte, S., accompanying paper, this issue.
(23) Groenenboom, G. C.; Meijer, A. J. H. M. *J. Chem. Phys.* **1994**, *101*, 7592
(24) Meijer, A. J. H. M.; Groenenboom, G. C.; Van der Avoird, A. *J. Chem. Phys.* **1994**, *101*, 7603.
(25) Meijer, A. J. H. M.; Groenenboom, G. C.; Van der Avoird, A. *J. Chem. Phys.* **1966**, *105*, 2247.
(26) Menzinger, M. *Selectivity in Chemical Reactions*; Whitehead, J. C., Ed.; NATO ASI Series C; Kluwer Academic: Dordrecht, 1988; Vol. 245, p 457.
(27) Menzinger, M. *Polon. Phys. Acta* **1988**, *A73*, 85
(28) Rettner, C. T.; Zare, R. N. *J. Chem. Phys.* **1981**, *75*, 3636.
(29) Rettner, C. T.; Zare, R. N. *J. Chem. Phys.* **1982**, *77*, 2416.
(30) Soep, B.; Whitham, C. J.; Keller, A.; Visticot, J. P. *J. Chem. Soc. Faraday Trans.* **1991**, *91*, 191.
(31) Soep, B.; Abbès, S.; Keller, A.; Visticot, J. P. *J. Chem. Phys.* **1992**, *96*, 440.
(32) Husain, D.; Roberts, G. *J. Chem. Soc. Fraraday Trans.* 2 **1986**, *79*, 1265.
(33) Moran, T. F.; Flannery, M. R.; Cosby, P. C. *J. Chem. Phys.* **1974**, *61*, 1261.
(34) McCann, K. J.; Flannery, M. R. *J. Chem. Phys.* **1975**, *63*, 4695.
(35) Augustin, S. D.; Rabitz, H. *J. Chem. Phys.* **1978**, *69*, 4195.
(36) Moran, T. F.; McCann, K. J.; Cobb, M.; Borkman, R. F.; Flannery, M. R. *J. Chem. Phys.* **1981**, *74*, 2325.
(37) DePristo, A. E. *J. Chem. Phys.* **1983**, *78*, 1237.
(38) Billing, G. D. *Comp. Phys. Rep.* **1984**, *1*, 239.
(39) Billing, G. D. *Int. Rev. Phys. Chem.* **1994**, *13*, 309.
(40) Hertel, I. V. *Adv. Chem. Phys.* **1981**, *45*, 341.
(41) Levine, R. D.; Bernstein, R. B. *Chem. Phys. Lett.* **1984**, *105*, 467.
(42) Smith, I. W. M. *J. Chem. Educ.* **1982**, *59*, 9.
(43) Pollak, E.; Wyatt, R. E. *J. Chem. Phys.* **1983**, *78*, 4464.
(44) Janssen, M. H. M.; Stolte, S. *J. Phys. Chem.* **1987**, *91*, 5480.
(45) The NAG Fortran Library, Mark 16; The Numerical Algorithms Group Limited, Oxford, 1993.
(46) *ATMOL Program Package*. Saunders, V. R.; Guest, M. F., Daresbury Laboratory, Warrington, UK, Knowles, P. J., University of Sussex, UK, and local extensions by Wormer, P. E. S.; Hettema, H., University of Nijmegen.
(47) Schlegel, H. B.; Wolfe, S.; Bernardi, F. *J. Chem. Phys.* **1977**, *67*, 4194.
(48) Herzberg, G. *Molecular Spectra and Molecular Structure*; Krieger: Malabar, 1991; Vol. III.
(49) Hettema, H.; Wormer, P. E. S.; Thakkar, A. J. *Mol. Phys.* **1993**, *76*, 533.
(50) Wlodarzak, G.; Herlemont, F.; Demaison, J.; Fayt, A.; Lahaye, J. G. *J. Mol. Spectrosc.* **1985**, *112*, 401.
(51) Flygare, W. H.; Benson, R. C. *Mol. Phys.* **1971**, *20*, 225.
(52) Ieki, M.; Kumamoto, E.; Kawaguchi, K.; Yamada, C.; Tanaka, T.; Hirota, E. *J. Mol. Spectrosc.*, **1978**, *71*, 229.
(53) Furio, N.; Campbell, M. L.; Dagdigian, P. J. *J. Chem. Phys.* **1986**, *84*, 4332.
(54) Yuh, H-J.; Dagdigian, P. J. *J. Chem. Phys.* **1984**, *81*, 2375.

JP961584N